Novel miniature motors with lateral stator for a wide torque and speed range

A. Tüysüz, A. Looser, and J.W. Kolar
Power Electronic Systems Laboratory
ETH Zurich
CH-8092 Zurich, Switzerland
tuysuz@lem.ee.ethz.ch

C. Zwyssig
Celeroton AG
Technoparkstrasse 1
CH-8005 Zurich, Switzerland
christof.zwyssig@celeroton.com

Abstract – **For various drilling applications where the space in the tool head is limited, two motor topologies with the stator outsourced from the head are proposed, allowing for compact design and direct drive. In order to meet the high torque requirements at low speed and operate at high speed up to 200 000 rpm a finite element analysis (FEA) is carried out and the machine design is optimized for maximum torque while considering the space limitations and the loss constraints at the critical operating points. As an example, for the specifications of a high-speed micro-machining spindle covering a wide application range, FEA results are presented. Moreover, a torque ripple compensation method based on phase current profiles obtained from FEA is proposed to eliminate the torque ripple caused by the stator asymmetry and slotting.**

I. INTRODUCTION

Recently, several electrical high speed motor drives have been reported in literature with speeds exceeding 100 000 rpm and power levels from 100 W up to several kWs. Typical applications are turbocompressors [1], gas turbines [2], [3] and machining spindles [4]. For different high-speed applications a 2 kW, 200 000 rpm machine is designed, optimized and tested in [5], the same specifications are mentioned in [6], and a 100 W, 500 000 rpm drive system is described in [7]. An overview of ultra-high-speed drive systems is given in [8], and the speed limits of high-speed electrical machines are determined in [9] and [10].

All the applications described above have one working point with a maximum speed and a maximum power requirement. The motors are, therefore, designed and optimized for this maximum speed and power. For the typical high-speed applications, turbocompressors, this is justified. However, there are high-speed applications that have different torque and speed requirements. The trend in micromachining is towards smaller tools requiring higher rotational speeds but lower torque. However, the same spindle still has to be able to drive larger tools requiring more torque at lower speeds. As an example, micro-machining spindles are developed for high-speed milling with tool diameters down to 0.1 mm, usually requiring almost zero torque at high-speed [11], whereas the same spindle should also be applied for thread cutting at very low speeds but with a high torque demand. For the watch industry and manufacturing of tooth crowns, new desktop machining centers are developed in order to process very small work pieces.

Another application with similar requirements is dental handpieces. Currently, different handpieces are used for different treatments, usually requiring low torque at high speed and high torque at low speed. Accordingly, there are activities to replace several handpieces with low-speed motors and step-up gearboxes for distinct applications with a single handpiece with a direct drive motor covering a larger torque and speed range.

Further applications with similar requirements are hand power tools such as hand held sanding machines.

The preferred motor topology for high-speed operation is the slotless permanent magnet machine [12]. This machine type has a constant torque-speed characteristic, and the torque can only be increased with increasing the machine volume (for constant relative losses). This is usually disadvantageous because many applications require a small size in order not to compromise the handling flexibility, e.g., in desktop micro-machining centers the space for the milling spindle is very limited and the head size of a spindle limits the possible shapes of the work piece. Similarly, the head size of a dental handpiece influences the ergonomics for the patient and the dentist. Furthermore, the diameter and length of the rotor limits the maximum rotational speed due to mechanical stress and rotordynamic constraints [9], [10].

This paper describes two novel motor topologies overcoming the drawbacks of the present high-speed motors, i.e., allowing for both high torque low speed and low torque high speed operation, with a small head size around the rotor. The topologies are shown in Fig.1. The main idea is to separate the rotor that generates the torque from the windings that generate the armature field. Firstly, the specifications for a typical application, a micro-machining spindle, are set and the concept of the novel motor topologies is described. Secondly, the motors are analyzed with parametric FEA, in order to find the optimal machine geometry. Finally, a torque ripple compensation method is proposed.

II. NOVEL MOTOR TOPOLOGIES

A. Specifications

Trends in micro-machining applications show speeds from almost zero speed up to 200 000 rpm. The torque for the high-speed drilling and milling is very low, while a torque of

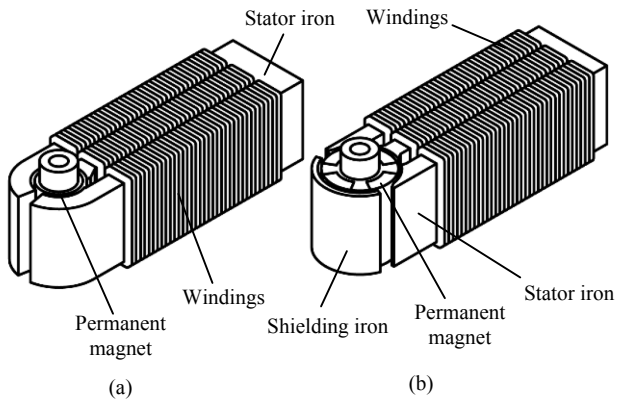

Fig. 1. Two novel lateral stator motor topologies: Motor with surrounding stator (a) and with section stator (b).

3 mNm is set as minimum for the low-speed applications with the goal of maximizing the torque at low speed. In order to machine very small work pieces (e.g. for the watch industry) the head of a machining spindle has a limited diameter and height (both set to 8 mm in this paper, see Fig. 2 and Table I), and the motor is allowed to grow only in one lateral direction if direct drive is to be used. Therefore, the two specifications related to the novel motor topologies described in this paper are: the high torque demand at low speed and the limited space available for the head of the motor. For further analysis in this paper, the geometrical constraints are set according to Fig. 2. The torque and speed requirements are summarized in two working points: low torque at high speed and high torque at low speed.

At high speed, the torque demand of most of the applications can be covered generating negligible amount of copper losses (P_{Cu}). Therefore, only the no-load losses ($P_{\mathrm{no\text{-}load}}$) are responsible for the heating and have to be limited according to the thermal design. Depending on previous experience on machines of similar size, the no-load loss limit is set to 1.2 W at the rated high-speed operating point of 200 000 rpm for the analysis in this paper. On the other hand, at low speeds all losses except for the dc copper losses can be neglected. As the maximum torque is usually applied only for a short time, the allowed copper losses ($P_{\mathrm{Cu,max}}$) are set to 8 W at this operating point. The machine optimization objective is to maximize the average torque over one rotation for the allowed copper losses at low speed considering the mentioned constraints. The torque and speed requirements as well as the loss limits are shown in Fig. 3.

B. Scaling of PM machines

In [9] and [10], scaling laws for high speed electrical machines are collected. They are all based on Esson's law

$$P = T\omega = Cd_r^2 l_a \omega \qquad (1)$$

where d_r is the rotor diameter, l_a is the active length and ω is the rotational speed. Esson's utilization factor C is dependent on the machine type, and various other variables such as the cooling system and size of the machine. In [13], a similar consideration is presented using empirical data for

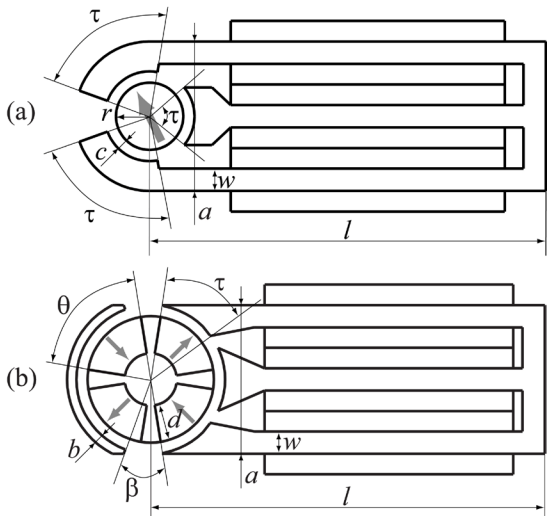

Fig. 2. Cross-section and parameter definition for the two novel lateral stator motor topologies: Motor with surrounding stator teeth (a) and with section stator teeth (b). The gray arrows indicate the magnetization direction of the permanent magnets.

torque and total volume for small permanent magnet machines. Therewith, the torque output of a machine can be estimated given the geometrical limitations. For a conventional permanent magnet machine that would fit in the geometric specifications described in this paper, the torque is estimated to be 0.24 mNm, which is more than a factor of 12 lower than the required torque of 3 mNm. Although this fact implies fitting a conventional permanent magnet machine into this limited space cannot generate the required torque, the empirical data used for scaling has no information about the losses, thus, no fair comparison could be made. Therefore, another step was taken, optimizing the usual motor topology used for these dimensions –the slotless permanent magnet motor– for highest torque according to [14] with the same geometric constraints and allowed copper losses of 8 W. This resulted in a maximum torque of 0.5 mNm, which is a factor of 6 lower than the required torque of 3 mNm.

Therefore, it can be concluded that standard symmetric round permanent magnet machines are no option for fulfilling the geometrical and torque requirements set in this paper, and novel topologies making use of the possibility to extend the stator in the direction of the handle have to be proposed.

C. Concept description

In Fig. 2, two possible designs of the lateral stator machine are given. The surrounding stator type machine in Fig. 2(a) is derived from a three-phase, two-pole electrical machine with three concentrated windings. The shape of the stator is modified such that the windings can be relocated from the area where the space is limited. By carrying the permanent magnet flux out of this restricted space, the stator can be made longer to gain more space for the windings. The section stator type machine depicted in Fig. 2 (b) is another type of lateral stator machine. In this configuration, a bigger rotor with four poles is used. Therefore, the torque can be increased compromising the simplicity of the rotor construction, as there is more space for permanent magnets and the number of poles is increased. Furthermore, the no-load losses of the

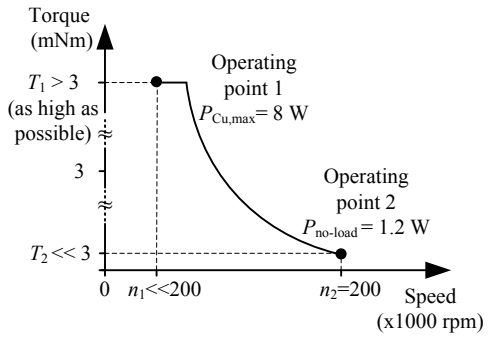

Fig. 3. Torque and speed requirements and loss limits.

section stator type machine are expected to be higher than those of the surrounding stator type machine because of the higher pole number causing higher iron losses and the larger rotor causing more air friction losses at the same speed. As the stator does not fully enclose the rotor in this configuration, a shielding iron is used to guide the magnetic field of the rotor magnets. Similar motor concepts have been presented in [15] and [16].

A major drawback of the lateral stator machines is the relatively high torque ripple resulting from the slotting and the nonsymmetrical configuration of the stator legs. Moreover, worsening of the torque ripple is observed at high load in FEA, as an effect of saturation in the teeth region and winding stray flux (flux leakage between the stator legs). Winding stray flux also negatively impacts the achievable average torque, limiting thereby the maximum extension of the stator length.

The stator is chosen to be built of iron based amorphous material because of its low losses and high saturation flux density. In order to meet the high torque-per-volume ratio, sintered rare earth magnets are used in the rotor. The shaft of the machine is not considered in this paper, as a non-magnetic retaining sleeve can be used around the rotor of the surrounding stator type machine which can also be used to transmit the torque to the load, and the shaft of the section stator type machine can be made of the same material as the rotor iron such that the shape of the shaft has no effect on the magnetic behavior of the machine.

III. FE Simulations

In [14] and [17] analytical models for evaluating the performance of machines with simple geometries are given. However, the partial saturation of the stator, the stray flux and the cogging torque play a big role in determining important performance criteria of the lateral stator machines, such as torque and iron losses. As these phenomena are not easy to model analytically on complex geometries, FE analysis is used to analyze the machines and to find the machine with the best performance. In this chapter, the modeling and optimization is described in detail.

A. Geometrical parameterization

For evaluating different possible machines and assessing the effect of specific geometric parameters to machine performance, the surrounding stator and the section stator type lateral stator machine geometries are parameterized as shown in Fig. 2, such that a set of parameters defines a unique machine. The parameters are summarized in Table I.

B. Loss models

1) Stator iron losses

Stator iron losses in electrical machines can be calculated using the empirical formula of Steinmetz. However, this method is developed for sinusoidal variation of magnetic flux density in time, and needs to be modified to be used for nonsinusoidal flux densities in the material. In [18], the modified Steinmetz equation (MSE), which can be used for nonsinusoidal flux densities, is developed. The MSE considers flux only in one direction, which is not exactly the case in the whole stator of the lateral stator machine. However, MSE is used to calculate the iron losses because the iron volume where a significant flux rotation occurs is much smaller than the iron volume where the flux is only one dimensional. Furthermore, the MSE does not need any additional data apart from the easily available Steinmetz coefficients.

2) Copper losses

As mentioned in the specifications, the machine has to produce relatively high torque at low speed, meaning that the fundamental-frequency copper losses are the only significant loss component at low speeds. Furthermore, at the rated speed of 200 000 rpm, the drive current frequency is 3.33 kHz for the surrounding stator type machine and 6.66 kHz for the section stator type machine. At those frequencies and using thin copper conductors, skin effect and proximity losses caused by the stray fields can be neglected and the total copper losses are given by

$$P_{\mathrm{Cu}} = \frac{3 \cdot \hat{J}^2 \cdot A_{\mathrm{w}} \cdot l_{\mathrm{w}} \cdot \rho_{\mathrm{Cu}}}{2 \cdot k_{\mathrm{f}}}, \tag{2}$$

for three-phase sinusoidal currents. $\hat{J}$ is the peak current density in a winding, ρ_{Cu} is the conductivity of copper and k_{f} is the copper filling factor. The parameters A_{w} and l_{w} are dependent on the parameters given in Table I. A_{w} represents the winding cross sectional area (i.e., area of one of the two adjacent rectangles between the stator legs in Fig. 2) and l_{w} represents the winding length (i.e., total length of the winding around one stator leg).

3) Air friction losses

In [14], it is shown that the air friction losses of a rotating cylinder in a fixed airgap can be calculated as

$$P_{\mathrm{air}} = c_{\mathrm{f}} \pi \rho_{\mathrm{air}} \omega^3 r^4 z, \tag{3}$$

where ρ_{air} is the density of air, ω is the angular speed, r is the radius and z is the length of the cylinder and c_{f} is the friction coefficient.

4) Rotor losses

Eddy currents are induced in solid conductive bodies in the rotor of an electrical machine, because of the time and space harmonics of the airgap field [19]. To analyze those eddy currents, a 3D transient FE simulation is needed, as the eddy current problem is a 3D problem [20]. As 3D FE simulations require much longer computational time than 2D simulations, there have been efforts to approximate the eddy current losses

using only 2D simulations, like in [20], [19] and [21]. These methods, however, either depend on assumptions like uniform magnetic field density over a magnet body [19] or involve additional calculation efforts creating an additional current sheet to account for the time and space harmonics of the airgap field ([21] and [20]).

Segmentation of the permanent magnets is widely used to reduce the eddy current losses. In this work, axially segmented permanent magnets were assumed in the rotor; therefore, eddy current losses in the rotor were not taken into consideration during the optimization progress. A 3D transient model of the optimum machine was later built and solved to compute the eddy current losses in the permanent magnets (section III.E).

C. Optimization method

After the machine topologies were geometrically parameterized as described in III.A, the parameter space was discretized according to Table I into parameter sets, each describing a unique machine design. Each of those parameter sets are then evaluated using 2D FEA. The advantage of such an exhaustive evaluation is that it is simple and there is no need of a predefined cost function definition, which would be the case when using state-of-the-art optimization techniques. Furthermore, it guarantees to find the global optimum in the discretized parameter space and yields data that are distributed over the entire parameter range, which allows for sensitivity analysis depending on any parameter and any performance criteria. The discretization steps are chosen relatively coarse at the first analysis, but still the results are good enough to make a fair comparison between surrounding stator and section type machines and to show which part of the parameter domain to look in order to find the best machine to fulfill the specifications.

Two finite element simulations are carried out for each machine parameter set. First, a machine design is simulated at zero speed and with a drive current producing 8 W copper loss, and then the same machine is simulated under no-load at the rated speed of 200 000 rpm. COMSOL Multiphysics simulation software package coupled with MATLAB is used for the simulation procedure. Two different routines are developed, one for zero speed and one for no-load simulations. In both of these routines, the rotor of the machine is rotated for one full electrical period (360° mechanical rotation for surrounding stator type and 180° mechanical rotation for section stator type) and magnetostatic computations are made for rotor positions in steps of 6° for both of the machines. In the zero speed simulation routine, the machine geometry is first created by picking the geometrical parameters from the parameter set defined in Table I. Then, depending on the machine geometry, the total winding area is calculated. Assuming a copper filling factor of 0.5, the peak current density that leads to the maximum short term allowed copper losses of 8 W is calculated using (2). Three-phase, 120^{o} phase shifted sinusoidal currents are assumed to be injected into the windings according to the instantaneous rotor position. Finally, the FE model is solved for each rotor position to obtain the torque characteristic over one full rotation. The torque is calculated both using Maxwell's stress tensor and virtual work principle in order to check any errors caused by FE related problems such as bad mesh.

TABLE I
DISCRETIZATION OF THE PARAMETER RANGE

Symbol	Parameter name	Values
Surrounding stator type		
τ	stator shoe span	60, 70, 80, 90, 100, 110 (degrees)
r	rotor radius	1.5, 2, 2.8 (mm)
c	airgap	0.6, 0.8, 1 (mm)
w	stator leg thickness	0.8 1.2 1.6 1.8 (mm)
l	stator length	20, 35, 40, 60, 80 (mm)
a	head diameter	8 (mm)
h	model depth (active length)	8 (mm)
Section stator type		
τ	stator shoe span	40, 45, 50 (degrees)
w	stator leg thickness	0.8, 1.2, 1.6 (mm)
l	stator length	15, 20, 30 (mm)
a	head diameter	8 (mm)
b	shielding iron thickness	1 (mm)
β	shielding iron gap	5, 15, 25 (degrees)
d	magnet depth	1, 2, 2.5 (mm)
θ	magnet span	54, 72, 81 (degrees)
h	model depth (active length)	8 (mm)

In the no-load simulation routine, the computations are repeated for zero winding current and the flux density in the iron is saved for each rotor position. Iron losses are calculated in post processing using the modified Steinmetz equation (section III.B.1). The air friction losses are calculated using (3), and are added to the iron losses in order to get the total no-load losses.

D. Simulation results

In Fig. 4 and Fig. 5, the performance concerning no-load losses and average torque at 8 W copper losses of both the surrounding stator and section stator type machines in the parameter range is given. Notice that section stator type machines produce more torque for given copper losses and more no-load losses than surrounding stator type machines, as expected because of the reasons mentioned in II.C. All of the surrounding stator type machines in the parameter range stay below the 1.2 W no-load loss limit, whereas there are many section stator type machines in the parameter range which produce more no-load losses than allowed. However, if all the machines under the no-load loss limit are compared, it can be seen that the section stator type machine is superior in terms of output torque. Accordingly, this machine type is selected for further analysis.

It can be seen in Fig. 5 that there is a group of motors producing similar torque (marked with a circle). All those machines have a stator leg thickness of 1.2 mm, a stator length of 15 mm and a magnet span of 81°. The magnet depths of the machines in this group are either 2 mm or 2.5 mm. On the other hand, different stator span and shielding iron gap parameters only have small influence on the performance. Finally, the torque ripple (difference between maximum and minimum instantaneous torque) is changing between 3.4 mNm and 7.5 mNm in those machines.

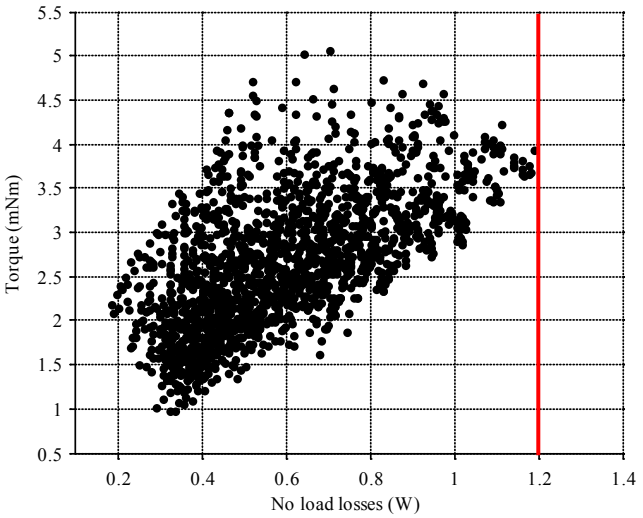

Fig. 4. Overview of the surrounding stator type motor performance concerning no-load losses and average torque. The red line denotes the 1.2 W no-load loss limit.

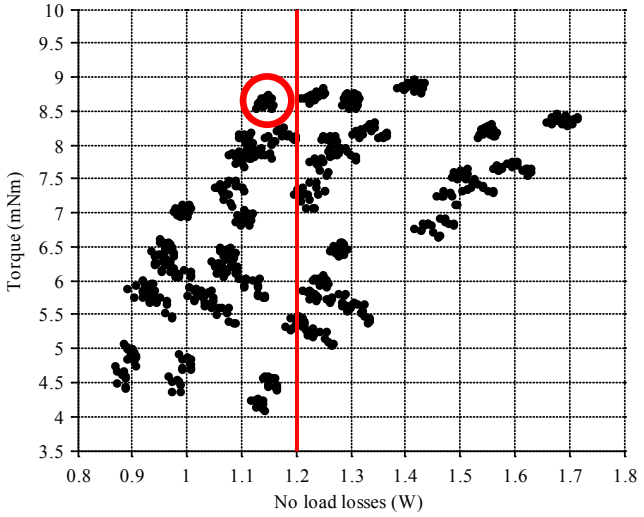

Fig. 5. Overview of the section stator type motor performance concerning no-load losses and average torque. The red line denotes the 1.2 W no-load loss limit.

Considering that all the machines in this group have similar average torques, and their no-load losses are all below the allowed limit, the best machine is chosen as the one with the minimum torque ripple. In Fig. 8, the torque of this selected machine is depicted under sinusoidal stator currents producing copper losses of 8 W. Table II shows the parameter set defining the selected machine.

E. Additional simulations on the selected machine

For the selected machine, Ansoft Maxwell was used to build and analyze 2D and 3D transient models for eddy current losses and phase inductance analysis.

1) Eddy current losses

Fig. 6 shows a snapshot of the 3D model that was used to estimate the eddy current losses in the permanent magnets.

As the eddy current losses increase proportional to the square of the rotational speed and stator currents are negligible at high speeds, in this work only the eddy currents that are induced due to the stator slotting are considered. In order to limit the eddy current losses in the magnets, each magnet is segmented into four pieces in the axial direction. As the iron parts are laminated, electrical conductivity is only assigned to the permanent magnets, which are electrically insulated from each other. At the maximum speed of 200 000 rpm, average of the total eddy current losses over one mechanical rotation is estimated as 140 mW and ignored as they are only a small percentage of the total no-load losses.

TABLE II
PARAMETER SET DEFINING THE BEST MACHINE

Symbol	Parameter name	Values
τ	stator shoe span	40 (degrees)
w	stator leg thickness	1.2 (mm)
l	stator length	15 (mm)
ϕ	head diameter	8 (mm)
b	Shielding iron thickness	1 (mm)
β	shielding iron gap	25 (degrees)
d	magnet depth	2 (mm)
θ	magnet span	81 (degrees)
z	model depth (active length)	8 (mm)

2) Phase inductance

Position sensors are not well suited for the application areas of dental drills and machining spindles mainly for reasons of space limitation but also for reasons of reliability, as the position sensors have to withstand the thermal cycles in regular vapor sterilization or the rough environment in machining centers. Therefore, the possibility of a self-sensing control method is investigated. In [22], it is shown that if the stator inductance of a machine varies with rotor position, the inductance can be monitored to track the rotor position. In Fig. 7, the stator inductances of the machine are plotted over rotor position, under no-load condition. It can be seen that there is a significant dependency of the phase inductances on the rotor position, which allows for the application of known position sensorless control methods.

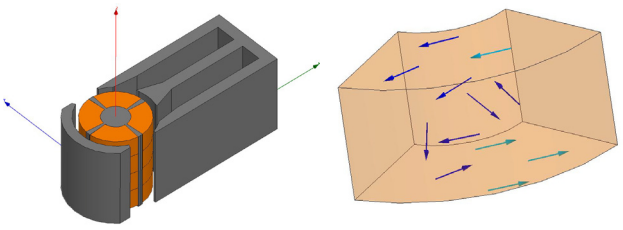

(a) (b)

Fig. 6. (a) Snapshot of the 3D model of the best machine. The windings are not modeled as only the no-load eddy current losses are investigated. (b) Instantaneous eddy currents in one single permanent magnet segment, arrows not drawn to scale.

IV. ACTIVE TORQUE RIPPLE COMPENSATION

Torque ripple is a much undesired effect in applications like machining spindles and dental drills, especially at low speeds. In literature, several machine design methods are presented to minimize torque ripple [22]. Some of those methods, e.g. skewing, reduce the torque pulsation but decreases the average torque as well. Other methods like direction

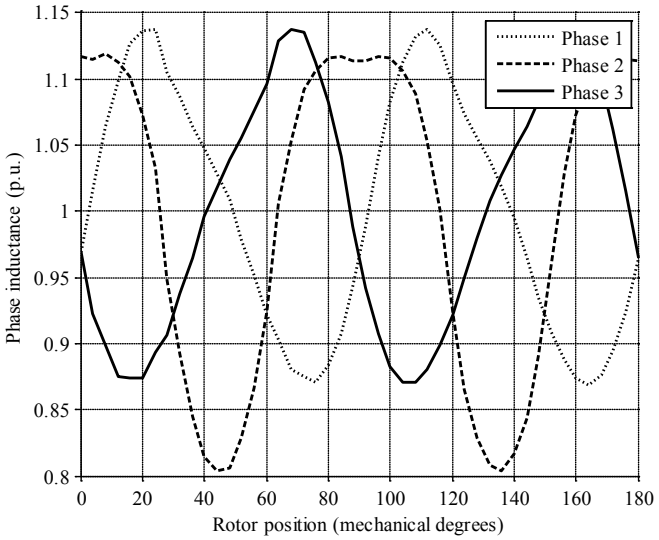

Fig. 7. Normalized phase inductances as function of rotor position.

dependently magnetized magnets may not be feasible with small sized rotors.

In literature, there are also various motor control methods, to reduce torque pulsations. In [24], an estimator based method is presented and in [25] the authors use the actual back EMF waveform to calculate the current waveform giving a ripple free torque. However, as the torque ripple in the machines described in this paper are load dependent and caused by phenomena that are not easy to model analytically, a FE based torque ripple compensation method is presented.

In order to find the stator currents that produce a ripple free torque, the optimized four pole machine (Table II) is simulated at fixed rotor positions ϕ for injected stator current density vectors:

$$\begin{aligned} j_{\mathrm{a}}(\varphi) &= \hat{J} \cdot \sin(2\phi + \delta), \\ j_{\mathrm{b}}(\varphi) &= \hat{J} \cdot \sin(2\phi + \delta + 120°), \\ j_{\mathrm{c}}(\varphi) &= \hat{J} \cdot \sin(2\phi + \delta - 120°), \end{aligned} \tag{4}$$

by sweeping the load angle δ from zero to 360° and $\hat{J}$ from the current density value producing 0.5 W copper losses up to the value producing 16 W, twice the allowed copper losses. Note that by sweeping $\hat{J}$ and δ all possible current vectors are covered in the given range for a star connected three-phase system. The torque obtained for one single rotor position is plotted in Fig. 10 as a function of the copper losses and the load angle. Finally, the three-phase currents yielding a constant torque over one electrical period are obtained from repeated sweep simulations for different rotor positions ϕ by selecting the current vector which produces the desired reference torque with minimal copper losses (Fig. 9). Given an accurate rotor position sensing and high bandwidth current control in order to inject desired current profiles, torque ripple compensation using the calculated current vectors can be achieved with such a machine.

The effect of the torque ripple is important at low speeds, and the described torque ripple compensation method is only considered to be used at low speeds. This also makes the

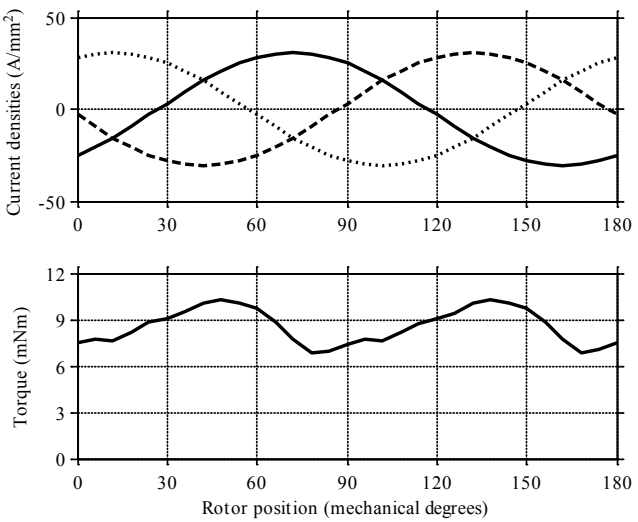

Fig. 8. Stator current densities and machine torque for sinusoidal currents creating a constant instantaneous copper loss of 8 W. Average torque is 8.6 mNm.

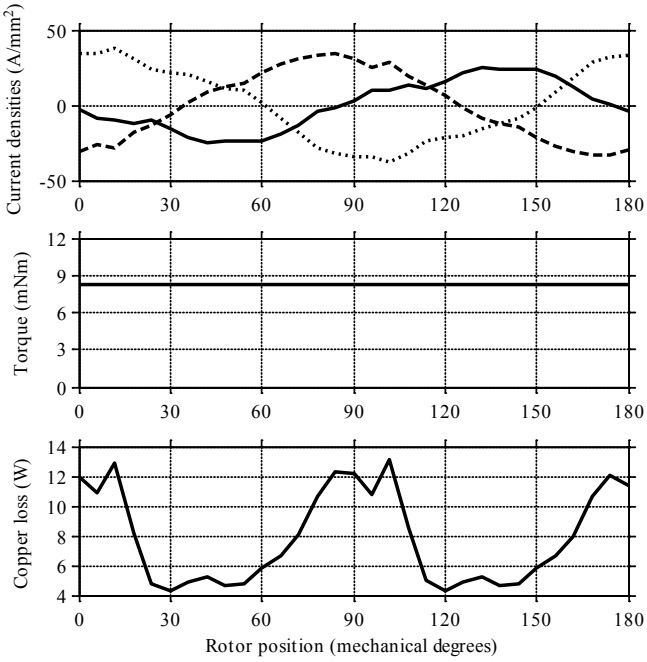

Fig. 9. Stator current densities, achievable machine torque and instantaneous copper losses for torque ripple compensation. Average copper losses are 8 W. Torque is constant at 8.2 mNm.

inverter design easier considering the high bandwidth current control. As mentioned in [7], block shaped currents are conventionally used to drive the machine at high speeds, and this can also be done with the lateral stator machines above the speed limit where the torque ripple can be tolerated. As the torque ripple compensation is considered only for low speeds, its effects on the iron losses are not investigated.

V. Conclusion

In drilling and machining applications with a wide speed and torque range where the space in the head of the tool is limited and mechanical transmission should be avoided, state-of-the-art permanent magnet motors cannot supply the

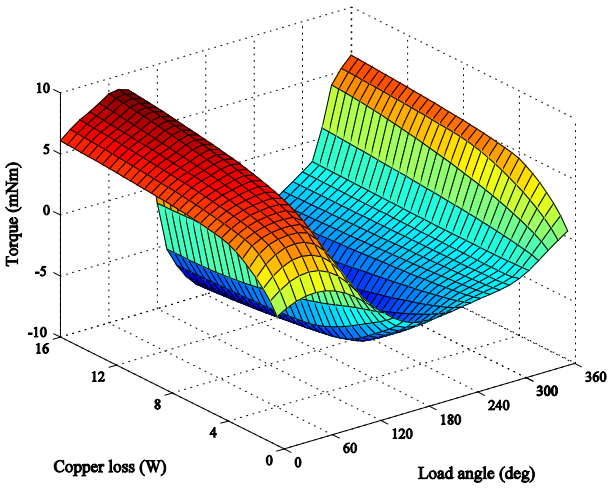

Fig. 10. Torque generated by different current vectors versus the copper losses and the load angle.

torque required at low speeds. Therefore, two novel motor topologies that fit in the head of the tool by outsourcing the stator to one lateral side are described in this paper.

Due to the complex geometry of the machines, a parametric FE analysis is undertaken allowing the selection of an ideal machine concerning torque and loss characteristics. A machining spindle was chosen as the target application, resulting in a motor that can supply 8.6 mNm torque at low speeds and has only 1.15 W of no-load losses at 200 000 rpm. Compared to a standard symmetric round high-speed permanent magnet motor which is optimized for efficiency and fits in the same head dimensions, the lateral stator machine produces 17 times more torque for the same copper losses of 8 W.

FE analysis shows that the torque waveform has a considerable amount of ripple for sinusoidal phase currents. Therefore, an FE analysis based active torque ripple compensation method is used to calculate the current waveform producing a ripple free torque.

The future work will focus on the experimental verification of the FE analysis and the self-sensing rotor position detection of the lateral stator machine. Furthermore, machine topologies with different stator phase numbers will be investigated.

REFERENCES

[1] D. Krähenbühl, C. Zwyssig, H. Weser, and J.W. Kolar, "A miniature, 500 000 rpm, electrically driven turbocompressor," *Energy Conversion Congress and Exposition, ECCE*, pp.3602-3608, Sept. 2009.

[2] D. Krähenbühl, C. Zwyssig, K. Bitterli, M. Imhof, and J.W. Kolar, "Evaluation of ultra-compact rectifiers for low power, high-speed, permanent-magnet generators," *35th Annual Conference of Ind. Electronics, IECON,* pp. 448-455, Nov. 2009.

[3] M. Morimoto, K. Aiba, T. Sakurai, A. Hoshino, and M. Fujiwara, "Position sensorless starting of super high-speed PM generator for micro gas turbine," *IEEE Trans. on Ind. Electron*., vol. 53, no. 2, pp. 415–420, Apr. 2006.

[4] I. Takahashi, T. Koganezawa, G. Su, and K. Ohyama, "A super high speed PM motor drive system by a quasi-current source inverter", *IEEE Trans. Ind. Appl.*, vol. 30, no. 3, pp. 683-690, May/June 1994.

[5] P. D. Pfister and Y. Perriard, "Very-high-speed slotless permanent-magnet motors: analytical modeling, optimization, design, and torque measurement methods," *IEEE Trans. on Ind. Electron.*, vol. 57, no. 1, pp. 296-303, Jan. 2010.

[6] L. Zhao, C. Ham, L. Zheng, T. Wu, K. Sundaram, J. Kapat, and L. Chow, "A highly efficient 200 000 rpm permanent-magnet motor system," *IEEE Trans. on Magn*., vol. 43, no. 6, pp. 2528–2530, June 2007.

[7] C. Zwyssig, S. D. Round, and J. W. Kolar, "An ultrahigh-speed, low power electrical drive system," *IEEE Trans. on Ind. Electron.*, vol. 55, no. 2, pp. 577 - 585, Feb. 2008.

[8] M. A. Rahman, A. Chiba, and T. Fukao, "Super high speed electrical machines – summary," in *Proc. of IEEE Power Engineering Society General Meeting*, vol. 2, pp. 1272-1275, June 2004.

[9] A. Binder and T. Schneider, "High-speed inverter-fed AC drives," *International Aegean Conference on Electrical Machines and Power Electronics, Electromotion*, Sept. 2007.

[10] A. Borisavljevic, H. Polinder, and J. A. Ferreira, "On the speed limits of permanent-magnet machines," *IEEE Trans. on Ind. Electron.*, vol. 57, no. 1, pp. 220-227, Jan. 2010.

[11] M. H. Kimman, H. H. Langen, J. van Eijk, and R. M. Schmidt, "Design and realization of a miniature spindle test setup with active magnetic bearings," *IEEE/ASME International Conference on Advanced Intelligent Mechatronics*, pp.1-6, Sept. 2007.

[12] N. Bianchi, S. Bolognani, and F. Luise, "Potentials and limits of highspeed PM motors," *IEEE Trans. Ind. Appl.*, vol. 40, no. 6, pp. 1570–1578, Nov./Dec. 2004.

[13] U. Kafader and J. Schulze, "Similarity relations in electromagnetic motors - limitations and consequences for the design of small dc motors," *9th International Conference on New Actuators*, *ACTUATOR*, pp. 309-312, June 2004.

[14] J. Luomi, C. Zwyssig, A. Looser, and J. W. Kolar, "Efficiency optimization of a 100 W 500 000 r/min permanent-magnet machine including air-friction losses," *IEEE Trans on Ind. Appl.,* vol.45, no.4, pp.1368-1377, Jul.-Aug. 2009.

[15] I. Hashimoto and T. Itoh, Japanese Patent JP9019123A, 1997.

[16] Y. Watanabe, Japanese Patent JP2000324775A, 2000.

[17] M. Markovic and Y. Perriard, "Simplified design methodology for a slotless brushless DC motor," *IEEE Trans. on Magn.,* vol.42, no.12, pp.3842-3846, Dec. 2006.

[18] J. Reinert, A. Brockmeyer, and R.W. De Doncker, "Calculation of losses in ferro- and ferrimagnetic materials based on the modified Steinmetz equation," *IEEE Trans. on Ind. Appl.,* vol.37, no.4, pp.1055-1061, Jul.-Aug. 2001.

[19] Z.Q. Zhu, K. Ng, N. Schofield, and D. Howe, "Analytical prediction of rotor eddy current loss in brushless machines equipped with surface-mounted permanent magnets, Part I: Magnetostatic field model," *5th International Conference on Electrical Machines and Systems, ICEMS,* vol. 2, pp.806-809, Aug. 2001.

[20] S. Ruoho, T. Santa-Nokki, J. Kolehmainen, and A. Arkkio, "Modeling magnet length in 2-D finite-element analysis of electric machines," *IEEE Trans. on Magn.,* vol. 45, no. 8, pp. 3114-3120, Aug. 2009.

[21] D.M. Saban and T.A. Lipo, "Hybrid approach for determining eddy-current losses in high-speed PM rotors," *IEEE International Electric Machines & Drives Conference, IEMDC*, vol. 1, pp. 658-661, May 2007.

[22] M. Schroedl, M. Hofer, and W. Staffler, "Sensorless control of PM synchronous motors in the whole speed range including standstill using a combined INFORM/EMF model," *12th International Power Electronics and Motion Control Conference, EPE-PEMC,* pp.1943-1949, 30. Aug. – 1. Sept. 2006

[23] J.F. Gieras, *Permanent magnet motor technology*, 3rd ed. Boca Raton, CRC Press, 2010.

[24] C. De Angelo, G. Bossio, G. Garcia, J. Solsona, and M.I. Valla, "Sensorless speed control of permanent magnet motors with torque ripple minimization" *28th Annual Conference of the Industrial Electronics Society, IECON*, vol.1, pp. 680- 685, Nov. 2002.

[25] S.J. Park, H.W. Park, Y.J. Lee, M. H. Lee, and C.U. Kim, "A new approach for pulsating torque minimization of brushless PM motor," *26th Annual Conference of the IEEE Ind. Electron. Society, IECON*, vol. 1, pp.76-82, 2000.